

# How Well Does Poisson–Boltzmann Implicit Solvent Agree with Explicit Solvent? A Quantitative Analysis

Chunhu Tan, Lijiang Yang, and Ray Luo\*

Department of Molecular Biology and Biochemistry, University of California, Irvine, California 92697-3900

Received: June 5, 2006; In Final Form: July 20, 2006

We have quantitatively studied the performance of a finite-difference Poisson–Boltzmann implicit solvent with respect to the TIP3P explicit solvent in a range of systems of biochemical interest. An overall agreement was found between the tested implicit and explicit solvents for hydrogen-bonding/salt-bridging dimers and peptide monomers and dimers of different conformations and different lengths. These comparative analyses also indicate a good transferability of empirically optimized parameters for the implicit solvent from small training molecules to large testing peptides. However, deviations between the two tested solvents are also apparent. Specifically, a consistent deviation was observed when hydrogen-bonding or salt-bridging dimers are within 4–6 Å. The deviation reaches a maximum at about 5.5 Å, the so-called water-bridging distance. The tested implicit solvent, even with optimized parameters, cannot capture the subtle fluctuation in the distance-dependent reaction field energy profiles, although smoothed profiles can still be obtained and are in overall agreement with those in the explicit solvent. Interestingly, the same mechanism underlining the above discrepancy is also responsible for the larger deviations of certain peptide conformations, such as parallel  $\beta$ -strand dimers. It is likely that the observed discrepancy may cause improper conformational distributions in simulations with the implicit solvent when hydrogen-bonding or salt-bridging interactions are crucial, such as secondary structure populations in proteins. Validation of the implicit solvent with optimized parameters in dynamics simulations will be the next step to study the influences of the observed discrepancy at biological conditions.

## 1. Introduction

As low-cost alternatives of explicit solvents, implicit solvents based on the Poisson–Boltzmann theory have become increasingly popular due to their computational efficiency and accuracy. In typical applications of the Poisson–Boltzmann theory,<sup>1,2</sup> including both numerical approaches<sup>3–5</sup> and analytical approximations,<sup>6–8</sup> solvent and any dissolved electrolyte are modeled by a structureless and continuous dielectric medium. Solute is usually represented in atomic detail with its atoms represented by spherical cavities and point charges at centers. The dielectric constant assigned for the space occupied by solute (e.g., proteins) is usually different from that assigned for the space occupied by solvent (e.g., water). Due to the finite size of solvent molecules, the union of solute atomic cavities is different from the space occupied by solute, i.e., the molecular cavity, which is a very complex function of solute atomic centers, atomic cavity radii, and solvent probe size.<sup>9</sup> A numerical procedure or an analytical approximation is often used to compute the molecular cavity. Once the molecular cavity is obtained, the dielectric constant inside and outside the molecular cavity can be assigned.<sup>9</sup> The electrostatic solvation energies (usually called reaction field energies) can be computed by solving the Poisson–Boltzmann equation.<sup>10,11</sup> The nonelectrostatic solvation energies are typically modeled with a term proportional to the solvent accessible surface area. In the present study, we will only focus on the electrostatic solvation energies.

A major advantage of Poisson–Boltzmann implicit solvents over explicit solvents is their high computational efficiency. However, it is worth asking how well the Poisson–Boltzmann implicit solvents agree with explicit solvents. Indeed, doubts

in the Poisson–Boltzmann theory were raised when these implicit solvents were applied in protein folding simulations of peptides,<sup>12,13</sup> though it was later reported that adjustment of atomic cavity radii were found to be able to alleviate many of the previously observed deficiencies.<sup>14,15</sup> Many more comparisons between the two different solvents were made in the past. In the study of Jeanchères et al.,<sup>16</sup> reaction field energies of 20 small molecules calculated by the finite-difference Poisson–Boltzmann method were compared to those calculated by the free energy perturbation method in the TIP4P explicit solvent. In the study of Marrone et al.,<sup>17</sup> the potentials of mean force for alanine dipeptide computed with both implicit and explicit solvents were compared. Recently, a comparison of atomic solvation forces was also reported with the hope to apply the implicit solvents in molecular dynamics simulations.<sup>18</sup> Whether agreement or disagreement was observed, a limitation in many previous comparisons was the lack of optimized atomic cavity radii for tested Poisson–Boltzmann solvents. Commonly in these studies, van der Waals radii in a force field were directly used to define the solute cavity boundary without optimization.

As is well-known, Poisson–Boltzmann reaction field energies depend sensitively on the solute cavity boundary, where the solvent-induced surface charge density is located. As mentioned above, the solute cavity is defined by solute atomic centers, atomic cavity radii, and solvent probe so that different reaction field energies computed with different cavity radii may have different agreements with explicit solvents. Thus, a set of accurate cavity radii is the basis for quantitative comparisons. To date, several sets of systemically optimized cavity radii have been presented.<sup>19–22</sup> In Sitkoff et al.,<sup>19</sup> atomic charges and radii

(PARSE) were obtained by modifying existing force field or quantum mechanically derived values, by fitting to experimental solvation energies of small organic molecules. Roux and co-workers<sup>20,21</sup> presented their optimized cavity radii, based on the molecular dynamics free energy simulations in explicit solvents. However, comparisons between explicit solvents and Poisson–Boltzmann implicit solvents with optimized cavity radii, especially when they were applied to biomolecules, had only been mentioned in Swanson et al.<sup>22</sup> In their study, Swanson et al. presented optimized cavity radii for amino acid templates in the AMBER force fields. Then the cavity radii were tested on four peptides. Reaction field energies calculated with both optimized and nonoptimized cavity radii were compared with those in the TIP3P explicit solvent, and a higher accuracy was observed when the optimized cavity radii were used, though deviations between implicit and explicit solvents were not further examined.

Different issues need to be addressed when such a quantitative comparison is performed. The first is the transferability of optimized cavity radii from small molecules (usually in the training set) to large molecules (usually biomolecules out of the training set). The cavity radii that we mentioned above are usually optimized based on the studies of small molecules. It is not guaranteed that they work well when applied to large and complex biomolecules. The second and more important issue is the influence of the different solvation treatments by implicit and explicit solvents. It is well-known that implicit solvents tend to break down where a discrete solvation description is required, such as individual structural water molecules interacting with functional groups. What remains unclear is whether a discrete solvation description is necessary for typical applications of implicit solvents where only solute–solute interactions are of interest. A quantitative study will help us to understand the limitation and scope of implicit solvents, at least for the electrostatic solvation effect as modeled by the Poisson–Boltzmann theory. The study will also help us develop more accurate implicit solvents.

In this study, we intend to address both issues as outlined above. Specifically, we are interested in the quality of a finite-difference numerical procedure (FDPB) as implemented in the PBSA program<sup>4,5</sup> in the AMBER8 distribution.<sup>23</sup> The explicit TIP3P solvent is used in the comparative analysis because of its rather good quality in reproducing experimental energetics.<sup>24</sup> The cavity radii are empirically optimized from the values reported previously.<sup>14</sup> The radii set of Swanson et al. for abrupt smoothed dielectric boundary definitions<sup>22</sup> are also used as reference. Here, the cavity radii are grouped by AMBER atom types and net charges of the templates to which the atoms belong to increase the ratio of parameters (cavity radii) and data constraints (reaction field energies). The current fitting effort is performed with nucleic acids included to further improve the ratio between parameters and constraints: a total of 42 reaction field energies for AMBER templates are used (29 amino acid side chain analogues, 5 bases, and 8 phosphate analogues of nucleic acids). Cavity radii for all single ions in the AMBER database are also computed and reported below. With this set of cavity radii, several biomolecular systems are studied to make quantitative comparisons between implicit and explicit solvents. These include reaction field energy profiles of hydrogen-bonding pairs and salt-bridging pairs and reaction field energies of helical and  $\beta$ -peptides.

In the following section, we first describe the molecular models used in this study, and then the computation details in both the explicit TIP3P solvent and the implicit FDPB solvent.

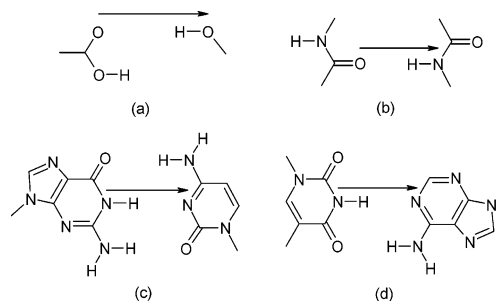


**Figure 1.** Tested hydrogen-bonding dimers. (a) ASH–SER. (b) NMA–NMA. (c) G–C. (d) A–T. The arrows indicate the directions of tested distance vectors separating each dimer. For each dimer, a total of 11 different conformations (distances) are tested, which are generated by keeping one molecule fixed and then moving away the other with 10 uniform steps. The step size is 0.5 Å.

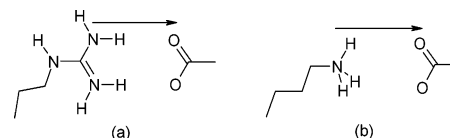


**Figure 2.** Tested salt-bridging dimers. (a) ARG–ASP. (b) LYS–ASP. See Figure 1 for more information on the setup of the tests.

In the Results and Discussion, we will compare the two solvents in various systems, discuss the sources of deviations, and comment on the transferability issue of cavity radii. Finally, Conclusions are presented.

## 2. Method

**2.1. Molecular Models.** Five groups of molecules studied in this paper are detailed here. These include the following: (1) small molecules in the training set; (2) hydrogen-bonding and salt-bridging dimers; (3) helical peptides ( $3_{10}$ -,  $\alpha$ -, and  $\pi$ -helices); (4)  $\beta$ -strand peptide dimers (anti- and parallel- $\beta$  pairs); (5) salt-bridge-containing helical peptides. All models were built in the XLEAP program of AMBER8.<sup>23</sup>

**2.1.1. Small Training Molecules.** There are 42 small molecules in the training set, including 25 amino acid side chain analogues (both neutral and charged), NMA (*n*-methylamine), and three dipeptides: GLY, ALA, and PRO; 5 bases (from five nucleotides: DA, DC, DG, DT, and RU, respectively); and 8 phosphate analogues with sugars (DAP from DA; DA3P from DA3, DA with a 3'-OH end group; DA5P from DA5, DA with a 5'-OH end group; DANP from DAN, DA with both 5'-OH and 3'-OH end groups; and their corresponding parts from RA, RA3, RA5, and RAN, respectively). These small molecules cover all the standard templates for proteins and nucleic acids in the AMBER force fields.

**2.1.2. Hydrogen-Bonding and Salt-Bridging Dimers.** ASH–SER (ASH = protonated aspartic acid), NMA–NMA, A–T, and G–C were used for hydrogen-bonding interactions. ARG–ASP and LYS–ASP were used for salt-bridging interactions. Their conformations are shown in Figures 1 and 2.

**2.1.3. Helical Peptides.** Three helical peptides, in  $3_{10}$ -,  $\alpha$ -, and  $\pi$ -conformations, respectively, were also studied. All of them were constructed in XLEAP starting from an ALA6 peptide (see Figure 3).

**2.1.4.  $\beta$ -Strand Dimers.** Both parallel and antiparallel  $\beta$ -strand dimers were studied. The backbone conformations were taken from the p53 DNA-binding core domain (pdb ID: 1TSR). The antiparallel dimer is built from residues 31–34 and 39–42; the parallel dimer is built from residues 233–236 and 372–375. All residues were mutated to alanines to expose the backbone

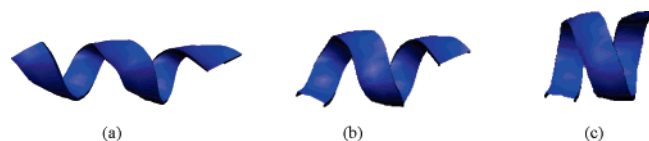


**Figure 3.** Three alanine-based helical peptides: (a).  $3_{10}$ -helix. (b)  $\alpha$ -helix. (c)  $\pi$ -helix. Each helix consists of six alanines.

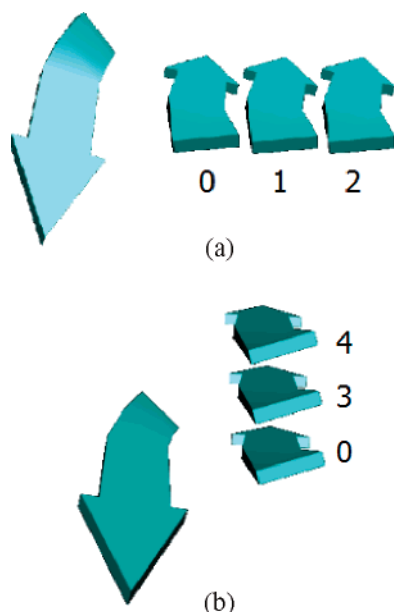


**Figure 4.** Five conformations of the antiparallel  $\beta$ -strand dimers. Position 0 is the native conformation. (a) Positions 1 and 2 are the two non-native positions with one strand moving to the right. (b) Positions 3 and 4 are the two non-native positions with one strand moving upward. The five conformations of the parallel  $\beta$ -strand dimers are set up similarly.

hydrogen bonds to solvent. For each dimer, five conformations were studied: one native and four non-native conformations. The non-native conformations were built by keeping the left strand fixed and moving the right strand two steps rightward and two steps upward, respectively. The step distance was 1 Å. Figure 4 shows the five conformations of the antiparallel dimer. The conformations of the parallel dimer were built similarly.

**2.1.5. Salt Bridge on Helical Peptides.** We also tested a set of larger biomolecules that contain a salt bridge to study the quality of the FDPB implicit solvent. Three 16-alanine  $\alpha$ -helical peptides with histidine (HIP, charged histidine) and aspartate (ASP) side chains were studied (see Figure 5). They were named HD2, HD3, and HD4 since HIP and ASP were separated by 3, 4, and 5 alanines, respectively.<sup>25,26</sup> It can be seen that a salt bridge exists between the two charged residues only in HD4. The sequences of these peptides are shown in Table 1.

**2.2. Simulation Details.** **2.2.1. Explicit Solvent Simulations.** All molecules in the present study were solvated by a TIP3P water box with a buffer of 11 Å in XLEAP. The system temperature was coupled to 300 K, and the system pressure was coupled to 1 bar by the Berendsen's coupling algorithms.<sup>27</sup> SHAKE was turned on for bonds containing hydrogen atoms<sup>28</sup> so that a time step of 2 fs was used for dynamics integration. Particle mesh Ewald with a real space cutoff of 9 Å was used for nonbonded interactions.<sup>29</sup> For easy comparison with implicit solvent calculations that were performed with rigid conformations, all solute atoms were restrained to their initial positions with a harmonic potential with a force constant of 50 kcal/mol·Å<sup>2</sup>. Before free energy simulations were started as discussed below, all systems were fully relaxed with the PMEMD program

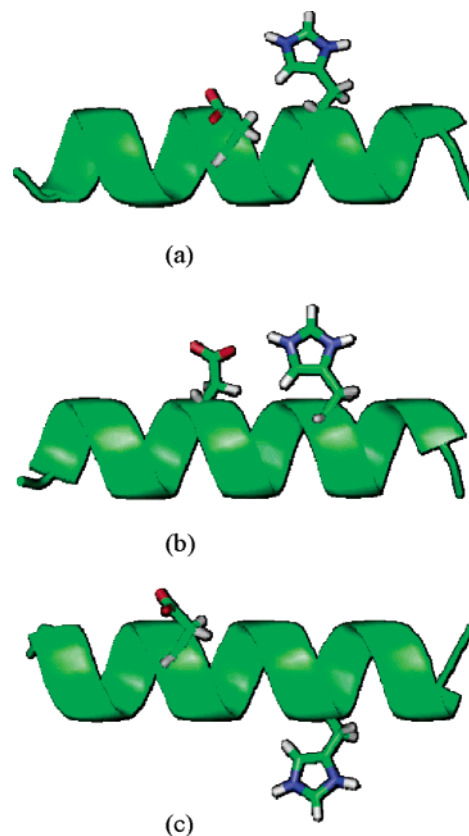


**Figure 5.** Three HIP/ASP-containing alanine 16-mers. See Table 1 for the sequences of the peptides. (a) HD3. (b) HD4. (c) HD5.

**TABLE 1: Sequences of Alanine-Based Peptides with Histidine (HIP) and Aspartate (ASP)**

peptide	sequence
HD3	AAAAHAADAAAAAA
HD4	AAAAHAAADAAAAAA
HD5	AAAAHAAAADAAAAAA

in AMBER8<sup>23</sup> for at least 4 ns or until there is no systematic drift in the running averaged potential energies.

Electrostatic charging free energies both in explicit solvent and in vacuum were calculated by the thermodynamic integration (TI) method:<sup>30</sup>

$$\Delta G = \int_0^1 \left\langle \frac{dH(\lambda)}{d\lambda} \right\rangle_\lambda d\lambda \quad (1)$$

where  $H$  is a parametrized Hamiltonian and  $\lambda$  is the coupling coefficient. In practice, the above integral is estimated by a numerical method, where the integrand is determined at a set of discrete  $\lambda$ 's (or "windows"). Here, the SANDER program in AMBER8 was used to compute the integrands. As only the electrostatic charging free energies were of interest, the Coulombic interaction between solute and solvent was decoupled by increasing  $\lambda$  from 0 to 1 in the step of  $\Delta\lambda$ . For small molecules in the training set,  $\Delta\lambda = 0.04$ , and for each  $\lambda$ , 40 ps molecular dynamics of equilibration ( $T_{\text{eq}} = 40$  ps) was ran, followed by another 40 ps of data collection ( $T_{\text{dc}} = 40$  ps). For larger systems outside the training set, such as hydrogen-bonding pairs and peptides,  $\Delta\lambda = 0.1$  and initial  $T_{\text{eq}}$  and  $T_{\text{dc}}$  were set to 100 ps. To guarantee convergence in free energies, the simulation times (both  $T_{\text{eq}}$  and  $T_{\text{dc}}$ ) were doubled until the free energies differed by less than 0.25 kcal/mol. The training molecules for which  $T_{\text{eq}}/T_{\text{dc}} \geq 160$  ps are needed to converge are listed in Table 2. The difference in the electrostatic charging free energies

**TABLE 2: Convergence of TI Simulated Reaction Field Energies for Training Molecules in TIP3P (kcal/mol) for Which  $T_{eq}/T_{dc} \geq 160$  ps/Å<sup>a</sup>**

template	40 ps/Å	80 ps/Å	160 ps/Å	320 ps/Å
ASP	-91.95	-92.25	-92.17	NA
CYM	-97.14	-96.87	-96.77	NA
DANP	-13.65	-13.95	-13.71	NA
DG	-22.96	-22.73	-22.85	NA
GLN	-12.14	-11.80	-11.80	NA
GLU	-92.43	-92.95	-92.58	-92.49
RA3P	-65.09	-65.70	-65.43	-65.50
RANP	-15.83	-16.06	-15.81	NA

<sup>a</sup> NA: simulation not performed because it is already converged with a shorter simulation time.

between solvated and in vacuo states is equivalent to the reaction field energy computed by FDPB.

The standard errors were used as statistical uncertainties for the free energies.<sup>31</sup> For each window in TI, the standard error of  $\langle dH/d\lambda \rangle$  is  $\langle \delta dH(\lambda)/d\lambda \rangle = (\sigma/\sqrt{N_e})$ .  $\sigma$  is the standard deviation of  $\langle dH/d\lambda \rangle$ .  $N_e$  is the “independent” sampling number, which can be calculated by the correlation time,  $\tau$ , of  $\langle dH/d\lambda \rangle$  and the data collection time  $T_{dc}$  as  $N_e = T_{dc}/(2\tau)$ .<sup>31</sup> Usually,  $\tau < 0.3$  ps for the training molecules, while  $0.4$  ps  $< \tau < 0.8$  ps for the larger testing molecules.

**2.2.2. Implicit Solvent Simulations.** The PBSA program in AMBER8 was used to calculate the reaction field energies using the numerical FDPB approach (termed PB below):<sup>4,5</sup>

$$\Delta G_{elec} = \frac{1}{2} \sum_j q_j \varphi_j \quad (2)$$

where  $j$  runs over all charged atoms. The reaction field potential  $\varphi_j$  at atomic charge  $q_j$  was computed by summation of dielectric boundary charges after solving the linearized form of the Poisson–Boltzmann equation:

$$\nabla \epsilon(\mathbf{r}) \varphi(\mathbf{r}) = -4\pi \rho(\mathbf{r}) - 4\pi \sum_i z_i c_i \exp[-z_i \varphi(\mathbf{r})/k_B T] \quad (3)$$

where  $\epsilon(\mathbf{r})$  is the dielectric constant,  $\varphi(\mathbf{r})$  is the electrostatic potential,  $\rho(\mathbf{r})$  is the solute charge,  $z_i$  is charge of ion type  $i$ ,  $c_i$  is the number density of ion type  $i$  far from solute,  $k_B$  is the Boltzmann constant, and  $T$  is temperature. Here, the summation is over all different ion types. The implicit solvent dielectric constant was set to 80, while the solute was set to 1. The boundary dielectric constants were assigned as the harmonic average of the solvent and solute dielectric constants.<sup>32</sup> The ion concentration was set to zero to be consistent with simulations in explicit solvent. The solvent-excluded surface was used to define the solute cavity, or the boundary of dielectric. The solvent probe radius was set as 1.6 Å, the  $\sigma$ -value of the TIP3P water. Grid spacing for the finite-difference solver was set to be 0.25 Å when the PBSA energies were shown to be well converged (much less than the free energy uncertainties in the explicit solvent simulations) with respect to the grid spacing (R. Luo, unpublished results). A two-level electrostatic focusing was used to speed up the assignment of electrostatic boundary condition. The coarse grid spacing was 2.0 Å. Grid charges assigned on the coarse grid were used to assign the boundary condition (i.e., boundary potential was computed as the sum of potentials of individual grid charges). The dimension of the coarse grid was set to be twice as large as the dimension of the solute to secure the quality of the nonperiodic boundary condition in PB calculations. To obtain grid-independent PB

**TABLE 3: Cavity Radii Based on the AMBER Atom Types<sup>a</sup>**

atom type	cavity radius (Å) (charge state)
Single Ions	
Li <sup>+</sup>	1.481
Na <sup>+</sup>	1.875
IP <sup>+</sup>	1.875
K <sup>+</sup>	2.288
Rb <sup>+</sup>	2.448
Cs <sup>+</sup>	2.712
F <sup>-</sup>	1.223
Cl <sup>-</sup>	1.516
IM <sup>-</sup>	1.815
Br <sup>-</sup>	1.745
I <sup>-</sup>	1.870
MG <sup>2+</sup>	1.515
CO <sup>2+</sup>	2.126
Zn <sup>2+</sup>	1.469
Heavy Atoms without Hydrogen Atoms	
CU	1.75 (neutral)
	1.85 (positive)
C	1.65 (negative)
	2.00 (neutral)
N/NB/NC/N*	1.75 (neutral)
O/O2	1.25 (negative)
	1.57 (neutral)
OS	1.30 (negative/neutral)
S/SH	1.45 (negative)
	2.00 (neutral)
P	1.95 (negative)
Heavy Atoms with Hydrogen Atoms	
CT	2.10 (negative)
	2.25 (neutral)
	2.50 (positive)
CU	2.15 (neutral)
	2.65 (positive)
N3	1.80 (neutral)
N (with 1H)	1.95 (neutral)
N/N2 (with 2H)	2.10 (neutral)
N2/N3	2.50 (positive)
NA	2.13 (neutral)
	2.65 (positive)
OH (on linear/aliphatic C)	1.93 (neutral)
OH (on cyclic/aromatic C)	1.79 (neutral)
SH	2.30 (neutral)

<sup>a</sup> The net charge state of a template to which an atom type belongs is listed after its cavity radius. CU stands for all aromatic carbon types in AMBER. Listed type/charge combinations are only for those observed in the AMBER templates. The rmsd between the PB and TI reaction field energies is 0.33 kcal/mol for the 42 templates used in the fitting. Cavity radii of single ions are computed analytically using the Born formula and TI reaction field energies.

energy for each molecular system, 27 different random finite-difference grid origins were used. The average of the 27 results was taken as the reaction field energy of the system.

The cavity radii were empirically optimized starting from previously reported values.<sup>14</sup> The radii set of Swanson et al.<sup>22</sup> for abrupt smoothed dielectric definitions was also used as reference in this work, but the fitting was performed with nucleic acids included. A total of 42 training molecules as mentioned above were included in the fitting. The current fitting considered the fact that cavity radii strongly depend on net charges as observed by Hummer et al. in single ions.<sup>33</sup> The cavity radii based on AMBER atom types and charges are listed in Table 3. The fitting quality for the 42 training molecules is shown in Figure 6. For completeness, cavity radii for single ions in the



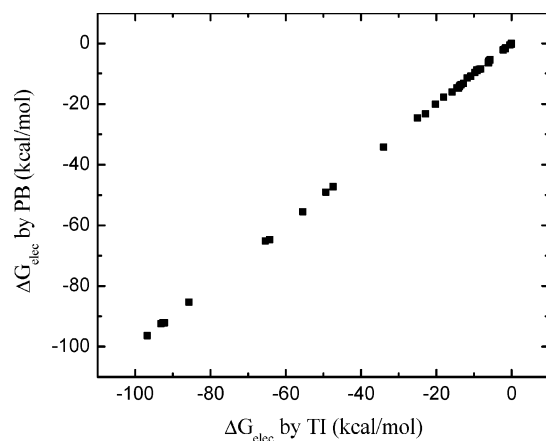


**Figure 6.** Correlation between TI and PB reaction field energies ( $\Delta G_{\text{elec}}$ ) for the 42 training templates. The correlation coefficient between the two sets of data is 0.99995; the rmsd is 0.33 kcal/mol.

AMBER database files were also computed according to the Born formula with the simulated reaction field energies in TIP3P.

### 3. Result and Discussion

**3.1. Hydrogen-Bonding and Salt-Bridging Dimers.** To compare the two solvents, reaction field energy profiles with respect to pairwise distance are studied for the six tested dimers. The results are shown in Figures 7 and 8. It can be seen that the overall correlation between the two solvents is very good, indicating a good transferability of the cavity radii from monomers to dimers. However, the difference between the two solvents is also noticeable: the PB free energy profiles are rather smooth, while the TIP3P free energy profiles of (TI) have local minima around 5.5 Å. The local free energy minimum can be explained by the so-called “water-bridged minimum”, which seems to appear first in Stofer et al.<sup>34</sup> Stofer et al. showed that, at the distance of the water-bridged minimum, water molecules can enter the gap between a tested base pair more frequently, forming linear and bridged hydrogen bonds with the two pairing bases. This results in a local minimum in the free energy profile.

Here, a further analysis of the NMA dimer is taken as an example to confirm this effect in our study. We calculated the average number density of water molecules within a cylindrical volume defined between O and H (see Figure 9). The average number density was computed over the last 1 ns of the equilibration run before the TI simulation. It was found that averaging over the last 2 ns of the run does not change the result noticeably, indicating the average number density has converged with respect to sampling time. The average number densities are plotted versus the pairwise distance between O and H in Figure 10. The uncertainties are in the order of  $10^{-5} \text{ 1/\AA}^3$ . When compared with Figure 7B, it is clear that more water molecules enter the gap at the distance around 5.5 Å, resulting in the observed local minima in the tested free energy profiles. A more detailed description of this phenomenon can be found in Figure 8 of Stofer et al.<sup>34</sup>

Water-bridged minima can also be found in other hydrogen-bonding dimers at almost the same distance. For the base pairs, the deviations are even larger (see Figure 7, parts C and D). The reason is simple: there are two or three hydrogen bonds between the bases. This indicates that deviations induced by water-bridged minimum are additive. A similar deviation also occurs in salt-bridging dimers (see Figure 8). However, the salt-bridging interactions themselves are so strong that the deviation

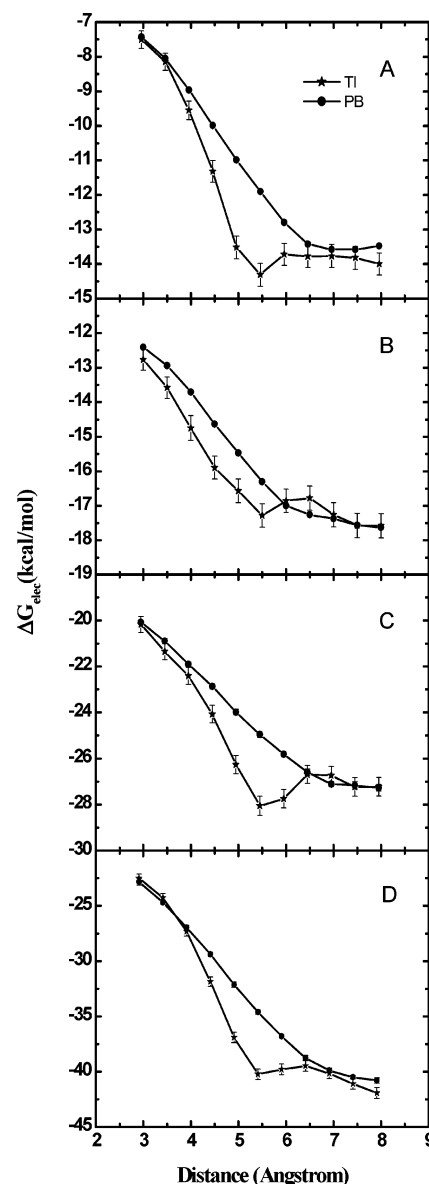


**Figure 7.** Reaction field energy ( $\Delta G_{\text{elec}}$ ) profiles of TI and PB with respect to the distance between two hydrogen-bonding molecules. (A) ASH-SER; rmsd = 1.20 kcal/mol. (B) NMA-NMA; rmsd = 0.66 kcal/mol. (C) A-T; rmsd = 1.37 kcal/mol. (D) G-C; rmsd = 2.55 kcal/mol.

from the water-bridged minimum is relatively small. Interestingly, the same water-bridging effect were also reported in Yu et al. in their study of salt-bridging ion pairs.<sup>35</sup>

From the above analyses, it is clear that deviation between the two tested solvents may occur in hydrogen-bonding conformations when the dimer distances are in the range of 4–6 Å, and the deviation reaches maximum at about 5.5 Å, the well-known water-bridging distance. The PB solvents cannot capture the subtle fluctuation in the free energy profiles even with a set of optimized cavity radii, although smoothed free energy profiles can still be obtained.

**3.2. Helices and  $\beta$ -Strands.** Next, the two solvents are applied to peptides. We first studied the conformation-dependent reaction field energies for helical peptides,  $3_{10}$ -,  $\alpha$ -, and  $\pi$ -helices. The reaction field energies calculated by explicit and implicit solvent are shown in Table 4. The data indicate that the reaction field energy of the  $3_{10}$ -helix is reproduced with the smallest deviation (relative error, 1.7%), while that of the  $\pi$ -helix

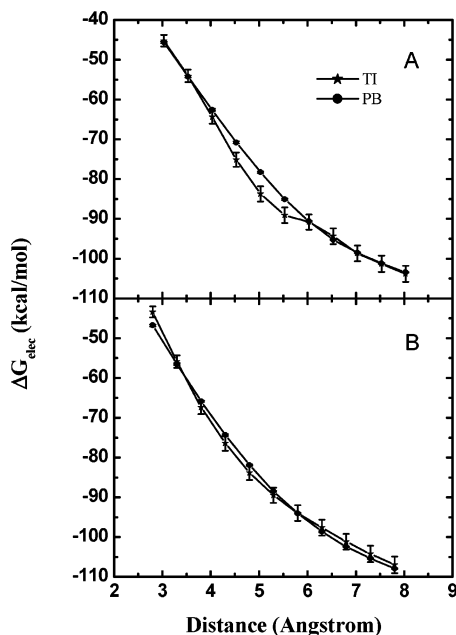


**Figure 8.** Reaction field energy ( $\Delta G_{\text{elec}}$ ) profiles of TI and PB with respect to the distance between two salt-bridging molecules. (A) ARG-ASP; rmsd = 2.50 kcal/mol. (B) LYS-ASP; rmsd = 1.60 kcal/mol.

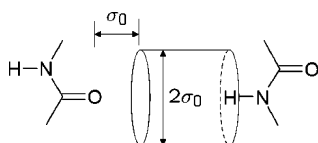


**Figure 9.** The cylindrical volume for the water number density calculation is defined between the peptide bond atoms O and H of the NMA dimer. Its radius is set as the van der Waals  $\sigma$  of O ( $\sigma_O = 1.48$  Å). Its height is set as the distance between H and O subtracted by  $\sigma_O$ .

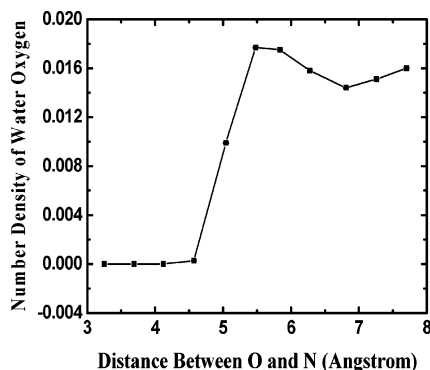


**Figure 10.** Number density of water oxygen ( $1/\text{\AA}^3$ ) with respect to the distance between the peptide bond atoms O and N of the NMA dimer. Around 5.5 Å, the number density reaches its peak value, which corresponds to the local minimum on the TI profile for the NMA dimer (see Figure 6). The uncertainties are in the range of  $10^{-5}$ , too small to be seen on the plot.

is the worst (relative error, 5.3%). The relative conformational energies between any two pairs of helices are also shown in Table 5.

We next studied the conformation-dependent reaction field energies for  $\beta$ -strand peptide dimers. The reaction field energies of all tested conformations can be found in Table 4. The relative reaction field energies between the native and modified conformations are listed in Table 6. Interestingly, the deviations of the antiparallel conformations are mostly smaller than those of the parallel conformations. This turns out to be caused by the water-bridging effect: the hydrogen-bonding distance in parallel

**TABLE 4: Reaction Field Energies of Tested Peptides by TI and PB<sup>a</sup>**

conformations	TI (kcal/mol)	PB (kcal/mol)	deviation (kcal/mol)
$3_{10}$ -helix	$-36.05 \pm 0.31$	$-35.48 \pm 0.03$	0.60
$\alpha$ -helix	$-45.20 \pm 0.35$	$-43.65 \pm 0.06$	1.55
$\pi$ -helix	$-56.48 \pm 0.44$	$-53.48 \pm 0.07$	3.00
antiparallel 0	$-32.61 \pm 0.32$	$-31.30 \pm 0.02$	1.31
antiparallel 1	$-36.32 \pm 0.45$	$-33.62 \pm 0.03$	2.70
antiparallel 2	$-44.05 \pm 0.43$	$-38.69 \pm 0.03$	5.36
antiparallel 3	$-34.49 \pm 0.38$	$-32.16 \pm 0.03$	2.33
antiparallel 4	$-38.34 \pm 0.45$	$-35.34 \pm 0.03$	3.00
parallel 0	$-32.00 \pm 0.39$	$-31.66 \pm 0.04$	0.34
parallel 1	$-36.96 \pm 0.38$	$-34.71 \pm 0.04$	2.25
parallel 2	$-46.47 \pm 0.53$	$-40.03 \pm 0.03$	6.44
parallel 3	$-33.63 \pm 0.39$	$-32.89 \pm 0.03$	0.74
parallel 4	$-39.20 \pm 0.45$	$-35.34 \pm 0.03$	3.86

<sup>a</sup> The deviations between the two solvents are shown in the last column. Antiparallel: antiparallel  $\beta$ -strand dimers. Parallel: parallel  $\beta$ -strand dimers. See text for explanations of the label numbers of the  $\beta$ -strand dimers.

**TABLE 5: Relative Reaction Field Energies of Helical Peptides by TI and PB and Their Deviations**

conformations	TI (kcal/mol)	PB (kcal/mol)	deviation (kcal/mol)
$3_{10}$ - to $\alpha$ -helix	-9.15	-8.17	0.98
$3_{10}$ - to $\pi$ -helix	-20.43	-18.00	2.43
$\alpha$ - to $\pi$ -helix	-11.28	-9.83	1.45

**TABLE 6: Relative Reaction Field Energies of  $\beta$ -Strand Dimers by TI and PB and Their Deviations**

conformations	TI (kcal/mol)	PB (kcal/mol)	deviation (kcal/mol)
antiparallel 0 to 1	3.71	2.32	1.39
antiparallel 0 to 2	11.44	7.39	4.05
antiparallel 0 to 3	1.88	0.86	1.02
antiparallel 0 to 4	5.73	4.04	1.69
parallel 0 to 1	4.96	3.05	1.91
parallel 0 to 2	14.47	8.37	6.10
parallel 0 to 3	1.63	1.23	0.40
parallel 0 to 4	7.20	3.68	3.52

**TABLE 7: Reaction Field Energies of Alanine 16-mers Calculated by TI and PB**

peptides	TI (kcal/mol)	PB (kcal/mol)	deviation (kcal/mol)
HD3	$-94.02 \pm 0.44$	$-92.57 \pm 0.11$	1.45
HD4	$-66.74 \pm 0.46$	$-69.20 \pm 0.11$	2.46
HD5	$-116.34 \pm 0.47$	$-116.23 \pm 0.08$	0.11

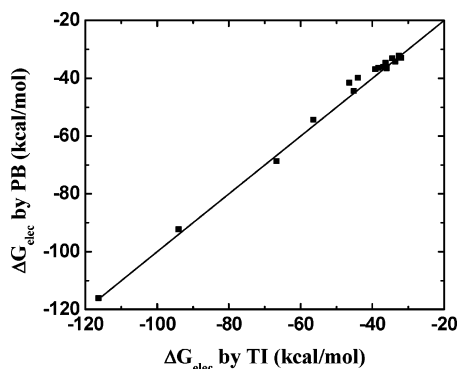
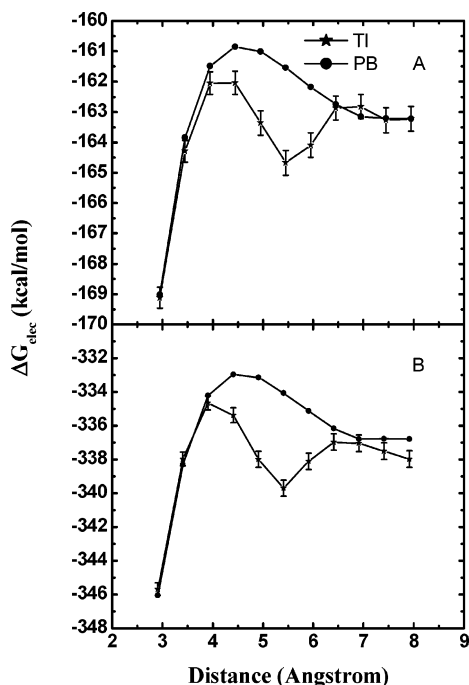
$\beta$ -strands (2.8–5.0 Å) is closer to the water-bridging distance (5.5 Å) than that in the antiparallel  $\beta$ -strands (2.6–4.7 Å). Figures 7 and 8 have shown that the deviation between explicit and implicit solvent is larger when the distance is closer to the water-bridging distance.

**3.3. Salt-Bridging on Peptides.** We further studied the performance of PB for a set of much larger systems. The results of TI and PB for the three tested systems can be found in Table 7. It is apparent that PB works well even for these longer peptides. Relative reaction field energies were also calculated and are shown in Table 8. The larger deviations for pairs involving HD4 are probably also due to the water-bridging effect between HIP and ASP.

Finally, Figure 11 shows an overall very good correlation between the two solvents for the conformations listed in Tables 4 and 7. The correlation coefficient is 0.997, indicating an

**TABLE 8: Relative Reaction Field Energies of Alanine 16-mers by TI and PB**

conformations	TI (kcal/mol)	PB (kcal/mol)	deviation (kcal/mol)
HD4–HD3	−27.28	−23.37	3.91
HD3–HD5	−22.32	−23.66	1.34
HD4–HD5	−49.60	−47.03	2.57

**Figure 11.** Reaction field energies ( $\Delta G_{\text{elec}}$ ) of 16 peptide conformations in Tables 2 and 5 calculated by TI and PB. The correlation coefficient between the two sets of data is 0.997; the rmsd is 2.90 kcal/mol.**Figure 12.** Electrostatic potential of mean force ( $\Delta G_{\text{elec}}$ ) of TI and PB with respect to the distance between two hydrogen-bonding bases. (A) A–T. (B) G–C.

overall good transferability of optimized cavity radii from small training molecules to larger and/or more complex molecular systems.

**3.4. Further Comments.** **3.4.1. Biological Implication of the Discrepancy at Water-Bridged Minimum.** To understand the biological implication of the observed discrepancy between PB and TI at the water-bridging distance, we have plotted the electrostatic potential of mean forces (summation of reaction field and Coulombic energies) for two hydrogen-bonding dimers, A–T and G–C, in Figure 12. Their full potentials of mean force were reported previously by Stofer et al.<sup>34</sup> When Figure 12 is compared with Figures 6 and 7 in Stofer et al.,<sup>34</sup> it is apparent that the water-bridging distance where the discrepancy between PB and TI occurs is the second minimum, while the hydrogen-

**TABLE 9: Two Sets of Cavity Radii (Å) and Their Corresponding Reaction Field Energies for the NMA Monomer by PB<sup>a</sup>**

radii set	CT(HC) <sub>3</sub>	CT(H1) <sub>3</sub>	N(H)	C	O	PB (kcal/mol)
1	2.60	2.60	1.95	2.40	1.36	9.17
2	2.25	2.25	1.95	2.00	1.57	9.04

<sup>a</sup> Set 2 is what we used in this study.

bonding distance is the first minimum. Interestingly, many structural water molecules in hydrogen-bonding networks are observed to be at the water-bridging distance in crystal structures, indicating that water-bridged minima are very common in biomolecules.<sup>36</sup>

**3.4.2. Transferability of Optimized Cavity Radii.** A major difficulty in fitting cavity radii is the insufficient constraints within the training molecules even if we have covered all templates in the AMBER force field database in this study. This is in part due to the high computational demand in obtaining converged free energies by TI in explicit solvent. The use of atom types and charge states in our fitting is to reduce the choices of cavity radii so that a higher ratio of constraints over parameters can be obtained. However, this is still not enough because there are over 20 atom types in the AMBER database. Quite often, there is only one case for a given atom type and charge state combination, for example, NZ in LYN (neutral lysine). Therefore, a transferability test outside the training set is essential. From Tables 4 and 7 we can conclude that the radii that we optimized in this study are transferable at least for the biomolecules studied here. However, the transferability of the optimized cavity radii to generic organic molecules might not be as good as observed here. More transferability tests need to be conducted before the cavity radii can be applied to generic organic molecules.

Even for applications to biomolecules, it occurred to us that even tests as shown in Tables 4 and 7 might not be enough. For example, in the study of hydrogen-bonding interactions in the NMA dimer, we found very sensitive dependence of reaction field energies upon cavity radii. During optimization, cavity radii for the following five (united) atoms need be determined for NMA: CT(HC)<sub>3</sub>, CT(H1)<sub>3</sub>, N(H), C, and O. Two sets of cavity radii of these atoms are listed in Table 9, where set 2 is what is used in this study. With each set of cavity radii, the NMA monomer reaction field energy in explicit solvent (9.14 kcal/mol) can be reproduced by PB with an absolute error of less than 0.1 kcal/mol (see Table 9). But when they are applied to study the reaction field energy profile of the NMA dimer, different agreements are observed. Figure 13 plots the two different PB reaction field energy profiles with the two sets of cavity radii. It is clear that both sets can reproduce the TI results with acceptable accuracy (absolute error less than 1.0 kcal/mol) when intermolecular distances are beyond 6 Å. However, for distances less than 6 Å, the results based on the two sets are apparently different. The first set obviously produces more positive results. These deviations can be explained by the unusually large radii of the three united carbon atoms. Surface visualization shows that the backbone carbonyl oxygen is almost covered by the united carbon atoms. The first set of radii does not affect the PB results when the two NMA molecules are completely separated. When they are in contact, the large united carbon atoms prevent more waters from interacting with the carbonyl oxygen in one NMA which forms a hydrogen bond with the amide nitrogen on the other NMA.

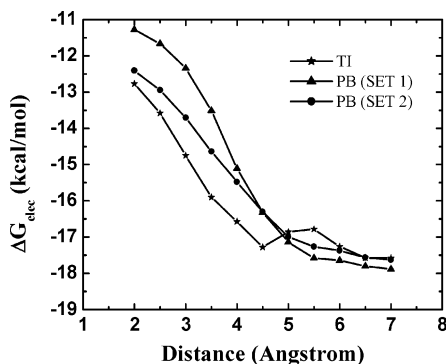


**Figure 13.** Reaction field energy ( $\Delta G_{\text{elec}}$ ) profiles (vs distance) of the NMA dimer computed with two sets of cavity radii as shown in Table 9. The rmsd of set (1) is 1.21 kcal/mol. The rmsd of set (2) is 0.66 kcal/mol. The uncertainties are the same as those for the NMA dimer in Figure 7 and are omitted here.

#### 4. Conclusions

In the present study, quantitative comparisons between a finite-difference Poisson–Boltzmann solvent and the TIP3P explicit solvent have been made for a series of molecular monomers and dimers of biochemical interest. In the studies of hydrogen-bonding/salt-bridging dimers and peptides of different conformations and different lengths, an overall agreement between the two solvents is observed. These comparative analyses also indicate a good transferability of the empirically optimized cavity radii from simple training molecules to complex and large biomolecules. It is found that transferability of cavity radii cannot be taken for granted. This is shown for two sets of radii with the NMA dimer as a test case.

However, deviation between the tested implicit solvent and explicit solvent is also noticeable. Specifically, a consistent deviation is found when hydrogen-bonding or salt-bridging dimers are within 4–6 Å. The deviation reaches the maximum near 5.5 Å, the so-called water-bridging distance. The tested finite-difference PB implicit solvent, even with a set of optimized cavity radii, cannot capture the subtle fluctuation in the reaction field energy profiles, although smoothed free energy profiles can be obtained and are in overall agreement with those in the explicit solvent. Interestingly, the same mechanism underlining the above discrepancy is also responsible for the larger deviations for parallel  $\beta$ -strand dimers between the two tested solvents.

It is possible to use a complex position-dependent dielectric constant near the solute to improve the agreement between PB solvents and explicit solvents because the local water density due to the water-bridging effect essentially produces a different dielectric response from that in the bulk water. It is also possible to develop more complex solvation treatments to incorporate a few explicit solvent molecules to overcome the limitations observed here, for example, as suggest by Yu et al.<sup>35</sup> Both directions would increase the computational complexity and cost of the PB framework.

Finally, how does the Poisson–Boltzmann implicit solvent perform in more complex biomolecules such as globular proteins under biological conditions? This question can only be answered by direct application of the implicit solvent in dynamics simulations of a wide range of biomolecules. Research efforts in this direction are currently underway in this group.

**Acknowledgment.** We thank Drs. M. K. Gilson and D. A. Case for critical reading of the manuscript. This work is supported in part by NIH GM069620.

#### Appendix

All optimized cavity radii for AMBER force fields have been released along with the Poisson–Boltzmann module in the AMBER9 package. Please contact the author for all data files used in the study.

#### References and Notes

- (1) Honig, B.; Sharp, K.; Yang, A. S. *J. Phys. Chem.* **1993**, *97*, 1101.
- (2) Honig, B.; Nicholls, A. *Science* **1995**, *268*, 1144.
- (3) Warwicker, J.; Watson, H. C. *J. Mol. Biol.* **1982**, *157*, 671.
- (4) Luo, R.; David, L.; Gilson, M. K. *J. Comput. Chem.* **2002**, *23*, 1244.
- (5) Lu, Q.; Luo, R. *J. Chem. Phys.* **2003**, *119*, 11035.
- (6) Still, W. C.; Tempczyk, A.; Hawley, R. C.; Hendrickson, T. J. *Am. Chem. Soc.* **1990**, *112*, 6127.
- (7) Tsui, V.; Case, D. A. *J. Am. Chem. Soc.* **2000**, *122*, 2489.
- (8) Onufriev, A.; Bashford, D.; Case, D. A. *Proteins: Struct., Funct., Bioinf.* **2004**, *55*, 383.
- (9) Gilson, M. K.; Sharp, K. A.; Honig, B. H. *J. Comput. Chem.* **1988**, *9*, 327.
- (10) Gilson, M. K.; Rashin, A.; Fine, R.; Honig, B. *J. Mol. Biol.* **1985**, *184*, 503.
- (11) Gilson, M. K.; Honig, B. *Proteins: Struct., Funct., Genet.* **1988**, *4*, 7.
- (12) Zhou, R. H.; Berne, B. J. *Proc. Natl. Acad. Sci. U.S.A.* **2002**, *99*, 12777.
- (13) Nymeyer, H.; Garcia, A. E. *Proc. Natl. Acad. Sci. U.S.A.* **2003**, *100*, 13934.
- (14) Lwin, T. Z.; Zhou, R. H.; Luo, R. *J. Chem. Phys.* **2006**, *124*, 34902.
- (15) Geney, R.; Layten, M.; Gomperts, R.; Hornak, V.; Simmerling, C. *J. Chem. Theory Comput.* **2006**, *2*, 115.
- (16) Jeanschales, A.; Nicholls, A.; Sharp, K.; Honig, B.; Tempczyk, A.; Hendrickson, T. F.; Still, W. C. *J. Am. Chem. Soc.* **1991**, *113*, 1454.
- (17) Marrone, T. J.; Gilson, M. K.; McCammon, J. A. *J. Phys. Chem.* **1996**, *100*, 1439.
- (18) Wagoner, J.; Baker, N. A. *J. Comput. Chem.* **2004**, *25*, 1623.
- (19) Sitkoff, D.; Sharp, K. A.; Honig, B. *J. Phys. Chem.* **1994**, *98*, 1978.
- (20) Banavali, N. K.; Roux, B. *J. Phys. Chem. B* **2002**, *106*, 11026.
- (21) Nina, M.; Beglov, D.; Roux, B. *J. Phys. Chem. B* **1997**, *101*, 5239.
- (22) Swanson, J. M. J.; Adcock, S. A.; McCammon, J. A. *J. Chem. Theory Comput.* **2005**, *1*, 484.
- (23) Case, D. A.; Darden, T. A.; Cheatham, T. E., III; Simmerling, C. L.; Wang, J.; Duke, R. E.; Luo, R.; Merz, K. M.; Wang, B.; Pearlman, D. A.; Crowley, M.; Brozell, S.; Tsui, V.; Gohlke, H.; Mongan, J.; Hornak, V.; Cui, G.; Beroza, P.; Schafmeister, C.; Caldwell, J. W.; Ross, W. S.; Kollman, P. A. *AMBER 8*; University of California: San Francisco, CA, 2004.
- (24) Jorgensen, W. L.; Chandrasekhar, J.; Madura, J. D.; Impey, R. W.; Klein, M. L. *J. Chem. Phys.* **1983**, *79*, 926.
- (25) Luo, R.; David, L.; Hung, H.; Devaney, J.; Gilson, M. K. *J. Phys. Chem. B* **1999**, *103*, 727.
- (26) Huyghues-Despointes, B. M. P.; Baldwin, R. L. *Biochemistry* **1997**, *36*, 1965.
- (27) Berendsen, H. J. C.; Postma, J. P. M.; Vangunsteren, W. F.; Dinola, A.; Haak, J. R. *J. Chem. Phys.* **1984**, *81*, 3684.
- (28) Ryckaert, J. P.; Ciccotti, G.; Berendsen, H. J. C. *J. Comput. Phys.* **1977**, *23*, 327.
- (29) Darden, T.; York, D.; Pedersen, L. *J. Chem. Phys.* **1993**, *98*, 10089.
- (30) Straatsma, T. P.; McCammon, J. A. *J. Chem. Phys.* **1991**, *95*, 1175.
- (31) Allen, M. P.; Tildesley, D. J. *Computer Simulation of Liquids*, 1989.
- (32) Davis, M. E.; McCammon, J. A. *J. Comput. Chem.* **1991**, *12*, 909.
- (33) Hummer, G.; Pratt, L. R.; Garcia, A. E. *J. Phys. Chem.* **1996**, *100*, 1206.
- (34) Stofor, E.; Chipot, C.; Lavery, R. *J. Am. Chem. Soc.* **1999**, *121*, 9503.
- (35) Yu, Z. Y.; Jacobson, M. P.; Josovitz, J.; Rapp, C. S.; Friesner, R. A. *J. Phys. Chem. B* **2004**, *108*, 6643.
- (36) Baker, E. N.; Hubbard, R. E. *Prog. Biophys. Mol. Biol.* **1984**, *44*, 97.